Available online at www.CivileJournal.org

# Civil Engineering Journal

(E-ISSN: 2476-3055; ISSN: 2676-6957)

Vol. 10, No. 07, July, 2024


# Bond-Slippage Characteristics between Carbon Fiber Reinforced Polymer Sheet and Heat-Damaged Geopolymer Concrete

Esmail A. Alshuqari [1*], Abdulkadir Çevik [1]

[1] *Department of Civil Engineering, Faculty of Engineering, Gaziantep University, 27310 Gaziantep, Turkey.*

Received 24 March 2024; Revised 16 June 2024; Accepted 24 June 2024; Published 01 July 2024

**Abstract**

The present study investigates the behavior of bond slip between carbon fiber reinforced polymer (CFRP) sheets and heat-damaged geopolymer concrete specimens that have been exposed to various elevated temperatures (20°C, 200°C, 400°C, and 600°C). The research aims to address the challenges posed by elevated temperatures on the bond strength and to highlight our original achievements in understanding and mitigating these effects. To assess the effect of different CFRP bonding widths and lengths, geopolymer concrete specimens were cast and bonded to sheets of CFRP. A total of 32 samples were tested under double-shear tension, examining the mechanical properties of geopolymer concrete, failure modes, bond force-slip curves, ultimate bond force and slip, stiffness, energy absorption, and scanning electron microscopy (SEM) analysis. The study found that temperatures up to 200°C caused a slight decline in mechanical properties and bond-slip behavior, with a 5% decrease in bond force and slippage. At 400°C, bond force and slippage reduced by 16%. Exposure to 600°C led to a significant 42% reduction in bond-slip behavior. The developed bond slippage model showed good agreement with experimental results, providing a valuable tool for predicting bond behavior under high-temperature conditions.

*Keywords:* Bond-Slip Behavior; Heat-Damaged Geopolymer Concrete; Carbon Fiber Reinforced Polymer (CFRP) Sheet; Elevated Temperatures.

## 1. Introduction

Because of its many advantages over other building materials, including its low cost, better fire resistance, flexibility, and ease of maintenance, concrete has been popular for ages [1]. The traditional binder used in the production of concrete is ordinary Portland cement (OPC). However, many environmental issues, such as global warming, can be attributed to the massive amounts of carbon dioxide released into the air during the cement production process [2, 3]. As the demand for environmental protection becomes more severe, numerous researchers are focusing their efforts on the creation of alternative materials to protect the global environment.

Geopolymer concrete, for instance, is an environmentally benign alternative material with long-term durability and sustainability. Geopolymer concrete is generally produced by activating aluminosilicate materials such as fly ash, slag, and metakaolin with alkali activators such as sodium hydroxide [4, 5]. Geopolymer concrete has received a lot of interest from researchers in recent years, and numerous studies have been conducted to examine and assess the mechanical and physical characteristics of normal and lightweight geopolymer concrete [6–9].

One of the most critical aspects influencing concrete properties is high exposure temperature. However, most studies have demonstrated that geopolymer concrete is more resistant to heat exposure than OPC concrete [10–13]. However, exposure of geopolymer concrete to high temperatures results in deterioration of the mechanical properties. Previous

* Corresponding author: alshogary88@gmail.com

http://dx.doi.org/10.28991/CEJ-2024-010-07-03

research indicates that when subjected to moderate temperatures up to up to 400 °C, the strength of geopolymer concrete declines somewhat but significantly when exposed to high temperatures up to around 600 °C [14–16].

The aforementioned makes it clear that effective repair methods would be required to restore structural capability and preserve the long-term durability of various structural parts, which have been extensively damaged by exposure to high temperatures. The most recent technique commonly utilized to repair and strengthen structural parts is carbon fiber-reinforced polymer (CFRP). Even though CFRP sheets are more expensive than traditional materials like steel, they have advantages over them, such as resistance to corrosive and chemical attacks, lightweight, high strength-to-weight ratio, low thermal conductivity, and simplicity of application [17–19].

One of the most efficient methods recommended for the external repair of reinforced concrete structures is externally bonding CFRP sheets to structural elements. This can be accomplished by bonding a suitable bond area of the CFRP sheets to well-prepared concrete substrates using an efficient epoxy. Thus, the quality of any structural element's repair is determined by the quality of the CFRP-substrate bonding. Several experiments have been carried out by researchers to examine the bond-slip behavior of several techniques, including near-surface mounted (NSM) bonding [20], embedding bars into geopolymer concrete [21–23], and external bonding using FRP sheets.

A bond-slip behavior was studied using the near-surface mounted (NSM) technique by Al-Abdwais [20]. The research involved testing geopolymer concrete prisms bonded with NSM CFRP laminates at various bond lengths, revealing significant bonding properties with an average bonding stress ranging from 8.97 to 15.58, depending on the bond length. The study highlighted the potential of combining geopolymer concrete with CFRP composites, demonstrating effective bonding through NSM techniques. Umesh [24] investigated the bond performance of normal and high-strength geopolymer concrete with Glass Fiber Reinforced Polymer (GFRP) bars. The study analyzed factors such as bar diameters, embedment lengths, and concrete grades on maximum pullout load and bond failure characteristics. It compared the adhesive and residual strengths of GFRP with steel specimens, highlighting GFRP's strong performance despite surface property differences. The research emphasized that higher concrete compressive strength enhances bond strength, showing improvements ranging from 14.57% to 32.12%.

The bond performance between FRP bars and geopolymer concrete under elevated temperatures was investigated by Zhao et al. [25]. The study found that bond strength initially increases but decreases as temperatures rise. Key factors influencing bond performance include temperature, FRP bar surface treatment, fiber type, and concrete strength. Results indicate bond retention ranges from 56.0% to 83.3% at 350°C, dropping to 17.7% at 400°C. The findings showed that FRP bars embedded in geopolymer concrete exhibit superior performance compared to those in ordinary concrete from 25°C to 350°C. On the other hand, researchers have conducted numerous experiments to evaluate the bond-slip behavior between conventional concrete and CFRP sheets. These experiments have been focused on many factors, such as the effect of concrete compressive and tensile strength [26, 27], the length and width of CFRP sheets [28, 29], the epoxy properties [30, 31], the addition of fiber to concrete [32], the type of surface preparation [33], and the anchorage system [34, 35].

The effect of elevated temperatures on the bond-slip behavior of OPC normal and lightweight concrete and CFRP sheet was examined by Haddad et al. [36]. According to their findings, being exposed to temperatures up to 400-600 ℃ had an adverse impact on the bons-slip behavior, which decreased bond strength and increased the associated slippage. Furthermore, although the majority of studies examined the bond-slip behavior between FRP sheets and OPC concrete, only a small number of researchers studied the bond-slip behavior with geopolymer concrete.

Alshuqari & Çevik [37] investigated the bond-slip behavior of geopolymer concrete and different types of FRP sheets. They found that employing CFRP sheets produced better bond-slip behavior findings than other forms of FRP sheets. Moreover, the usage of the end-groove anchored system was beneficial for enhancing the bond force and preventing de-bonding at failure. Additionally, they claimed that geopolymer concrete had a better bond with CFRP sheets compared to conventional concrete. While previous research by Alshuqari & Çevik [37] explored the bond-slip behavior of geopolymer concrete with various FRP sheets at room temperature, a significant gap remains in our understanding of this behavior under elevated temperatures. This unexplored area requires thorough investigation to better understand how heat damage affects the interaction between CFRP sheets and geopolymer concrete.

This study aims to address this knowledge gap by providing a comprehensive analysis of bond-slippage characteristics between CFRP sheets and heat-damaged geopolymer concrete. This research is innovative as it specifically focuses on how high temperatures influence the bond-slip behavior, which is crucial for understanding the performance and durability of geopolymer concrete structures in high- temperature environments.

By filling this crucial gap in the literature, this study aims to provide valuable insights that will help improve the design and maintenance of geopolymer concrete structures exposed to high temperatures in various applications.

For this purpose, a total of 32 specimens with dimensions of 150×150×150 mm were used in an experimental program to evaluate the effect of different elevated temperatures (20℃, 200℃, 400℃, and 600℃), CFRP bonding width

Wf (50 and 100 mm), and CFRP bonding length Lf (50 and 100 mm). The geopolymer blocks were cast, heated to elevated temperatures, bonded to the appropriate CFRP sheets, and then tested through a double-shear test. As part of this study, the mechanical properties, the failure of mode, the bond force and slip, the effect of elevated temperatures on bond-slip properties, and the SEM analysis were examined for geopolymer concrete specimens.

## 2. Experimental Program

### 2.1. Description of Specimens

In this study, a total of 32 geopolymer concrete blocks with dimensions of 150 x 150 x 150 mm were cast. The geopolymer concrete specimens were divided into four groups depending on the temperature level. All tested specimens were labeled with letters and numbers that reflected the geopolymer concrete (NWG), temperature effect (T: 20, 200, 400, 600 °C), CFRP bonding width (Wf: 50 mm, 100 mm), and CFRP bonding length (Lf: 50 mm, 100 mm). A detailed description of the tested samples is presented in Table 1, and Figure 1 illustrates the flowchart for the research methodology.

**Table 1. Description of the testing procedure and specimen designation**

| Designation | Temperature (℃) | Bond width, Wf (mm) | Bond length, Lf (mm) | No. of specimens |
|---|---|---|---|---|
| NWGCT20°,200°,400°,600°Wf50Lf50 | 20, 200, 400, 600 | 50 | 50 | 8 |
| NWGCT20°,200°,400°,600°Wf50Lf100 | | 50 | 100 | 8 |
| NWGCT20°,200°,400°,600°Wf100Lf50 | | 100 | 50 | 8 |
| NWGCT20°,200°,400°,600°Wf100Lf100 | | 100 | 100 | 8 |

Note: during the test, two samples were used for each type of designation.

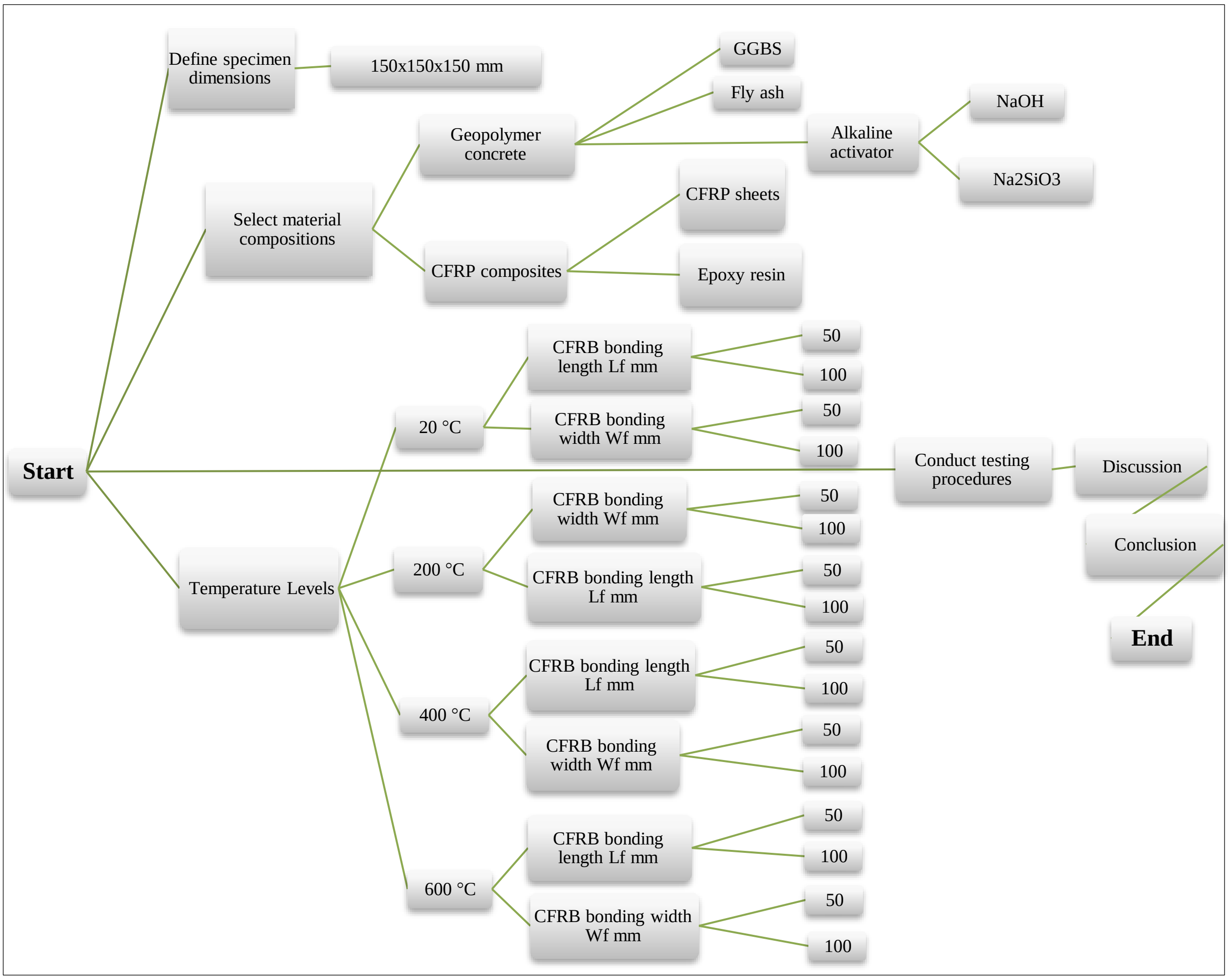


**Figure 1. Flowchart for the research methodology**

## 2.2. Material Properties

### 2.2.1. Geopolymer Concrete

In this research, the production of geopolymer specimens was achieved using ground granulated blast furnace slag (GGBS) and fly ash (FA). Table 2 shows the chemical characteristics of GGBS and fly ash. The alkaline activator used to activate the geopolymer binder was formed by blending sodium hydroxide solution (NaOH) with sodium silicate (Na2SiO3). The NaOH solution was made by dissolving sodium hydroxide powder in water with a concentration of 12 moles and then leaving it at room temperature for 24 hours before use. The sodium silicate solution contained 13.7% sodium dioxide, 29.4% silicon dioxide, and 55.5% water. The binder ratio of slag to fly ash was 1:2 for geopolymer concrete, and the alkaline activator solution to binder ratio was 0.5. A superplasticizer was added to achieve the desired workability of the mixtures. The samples were cast, covered for a day with plastic sheeting, and then demolded and sealed in plastic bags, kept at room temperature for 28 days. Table 3 shows the mix proportions of geopolymer concrete, and Figure 2 illustrates the mixing, casting, and curing processes for both samples.

**Table 2. Chemical Properties of Fly Ash, and GGBS**

| Component | $Al_2O_3$ % | MgO % | CaO % | $K_2O$ % | $Fe_2O_3$ % | $Na_2O$ % | $SO_3$ % | $SiO_2$ % | Specific gravity | Loss on ignition | Blaine fineness, $m^2/kg$ |
|---|---|---|---|---|---|---|---|---|---|---|---|
| Fly ash | 24.4 | 10.3 | 34.12 | 0.97 | 7.1 | 0.38 | 0.29 | 36.4 | 2.79 | 1.52 | 379 |
| GGBS | 10.39 | 2.4 | 2.24 | 3.37 | 0.69 | 0.35 | 0.49 | 57.2 | 2.15 | 1.64 | 418 |

**Table 3. Mixture proportions of geopolymer concrete ($Kg/m^3$)**

| $Na_2SiO_3$ | NaOH | Slag | Fly ash | Coarse Agg. | Fine Agg. | SP, % |
|---|---|---|---|---|---|---|
| 150 | 60 | 280 | 140 | 866 | 800 | 3 |

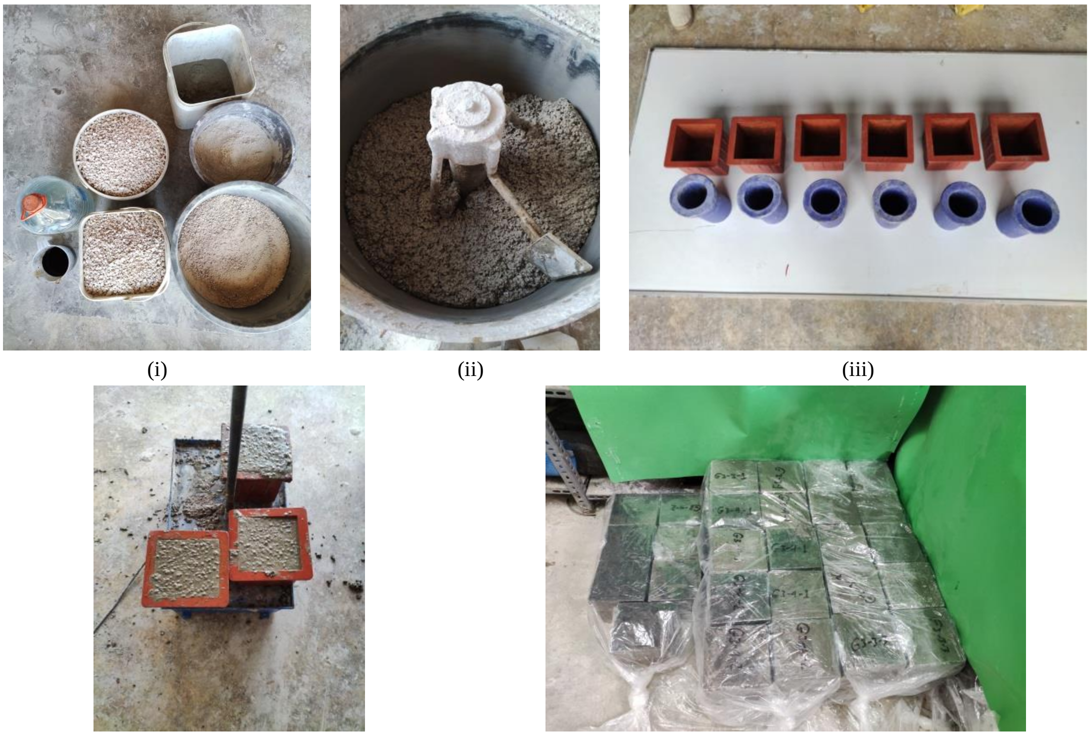

(i) (ii) (iii)

(iv) (v)

**Figure 2. Mixing, casting, and curing of the geopolymer concrete samples: (i) consistent ingredients; (ii) blending activator with geopolymer concrete; (iii) molds used for casting specimens; (iv) casting and vibration; (v) specimen curing**

### 2.2.2. CFRP sheet and the Epoxy Adhesive

In this study, a unidirectional CFRP sheet with a 0.3 mm thickness and epoxy resin were used for bonding with geopolymer concrete specimens. Table 4 summarizes the mechanical properties of CFRP and epoxy adhesive.

**Table 4. Properties of CFRP sheet and epoxy resin**

| Material type | Tensile strength, MPa | Modulus of elasticity, GPa | Thickness, mm | Elongation, % | Area weight, $g/m^2$ |
|---|---|---|---|---|---|
| CFRP | 4900 | 240 | 0.3 | 2.1 | 300 |
| Epoxy resin | 54 | 3.034 | - | 3.5 | - |

### 2.3. Heating Procedure

After the completion of curing, all samples that will be exposed to 200 °C, 400 °C, and 600 °C had previously been preheated at 105 °C for 24 h in an oven. This was done to eliminate surface moisture and dry the samples before applying the target temperature [38]. After the preheating process, the specimens were placed into an electric furnace and heated at a steady rate of 10 °C/min until the desired temperature was achieved. The specimens were then kept at a constant temperature for 2 hours to achieve a steady-state heat condition, as illustrated in Figure 3-b. At the end of the heating process, the specimens were left in the furnace to cool. Figure 3 illustrates the electric furnace used and the time-temperature schedule of the heating process.

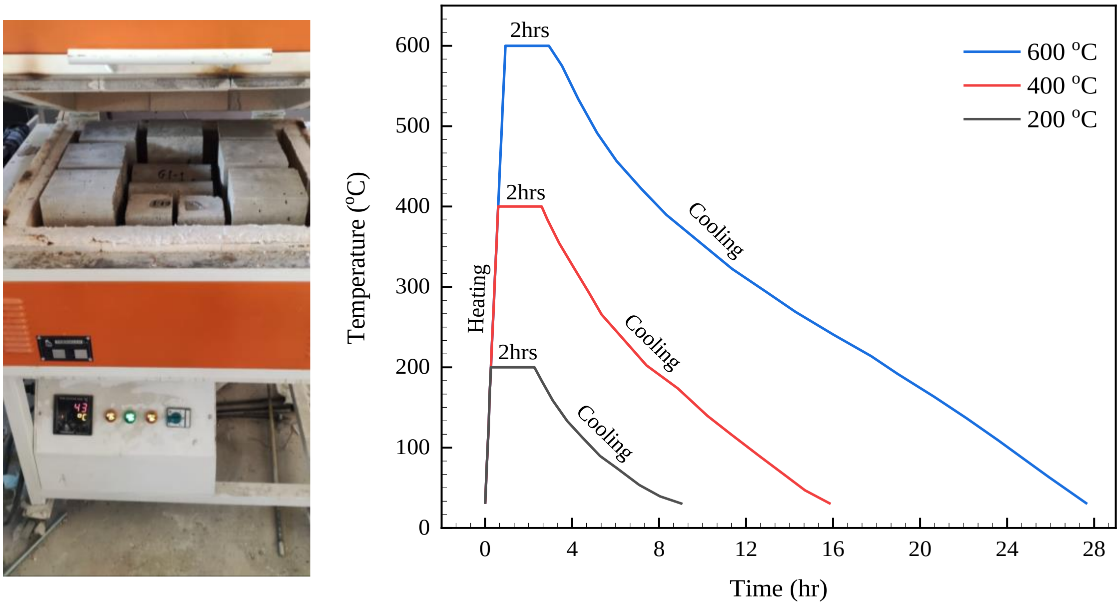


(a) (b)

**Figure 3. (a) Electric furnace, (b) The time-temperature schedule of heating process**

### 2.4. Preparation of Specimens

After the heating procedure, the heated and unheated specimens were prepared for bonding to CFRP sheet. To do this, the specimen's weak surface was first removed with a steel wire brush grinding equipment, followed by a cleaning with an air jet to clean up any leftover dust. prior to applying the epoxy resin, the area where the CFRP sheets would be bonded was marked, and the surrounding area was protected using plasterer's tape. Furthermore, a 25 mm of the specimen's top was left unbonded with plastering tape to avoid the possibility of a failure at a localized area due to stress concentration. Finally, epoxy resin was used to attach the CFRP sheet to both sides of the specimens, and the samples were left to cure for two weeks before testing.

### 2.5. Testing Procedures

#### 2.5.1. Bond-Slip Test

The bond-slip test procedure was used to evaluate the results of double shear tension testing on both heated and unheated samples. Two repetitions were used for each specimen, and the results were evaluated based on the average of these two samples. To perform the bond-slip test procedure, a specialized steel frame and fasteners were used to secure all test specimens to the lower platen of the testing machine. Figure 4 illustrates this setup. A hydraulic jack with a 100 KN capacity was used to apply the same tension load to all specimens. The test was conducted under displacement-controlled conditions, with a loading rate of 0.3 mm/min, and a load cell was used to measure the load. To determine the slip at the interface between the sample face and the CFRP sheet, two linear variable differential transformers (LVDTs) were placed on either side of the specimen. To mount the LVDTs, an L-shaped steel plate was affixed to the surface of the CFRP sheet. The data from the LVDTs and load cell were recorded using a data acquisition system.

#### 2.5.2. Mechanical Strengths

To assess the mechanical properties of geopolymer concrete, their compressive and splitting tensile strengths were examined as per ASTM C109 and ASTM C496 standards, respectively. Cube-shaped specimens measuring 150×150×150 mm were utilized for compression strength testing, while cylinder specimens measuring 100x200 mm were used to evaluate splitting tensile strength. Three samples from each group were tested, and the average strength was determined.

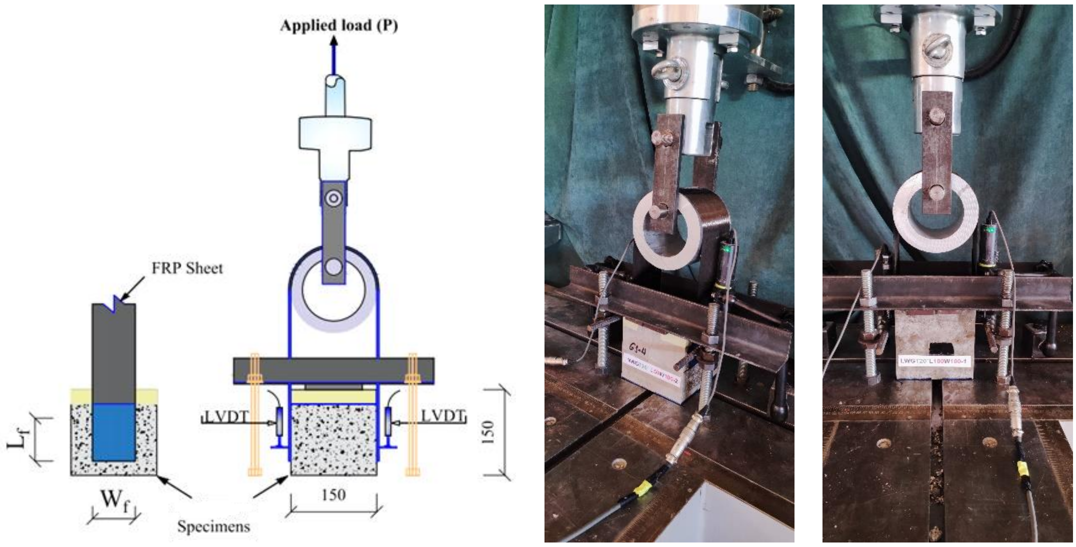


**Figure 4. Double-shear bond test setup**

## 3. Results and Discussion

### 3.1. Mechanical Properties of Geopolymer Concrete

The results of density, compressive, and splitting strength versus applied temperature for geopolymer concrete are summarized in Table 5. The relative residual density of specimens after exposure to elevated temperatures was plotted in Figure 5-a. The relative residual densities of geopolymer concrete specimens at 200 °C, 400 °C, and 600 °C were 98%, 95%, and 93% of the control specimen (unheated specimen), respectively. Figure 5-b displays the residual compressive strength versus applied temperature for geopolymer concrete specimens. In comparison to the unheated specimen, the residual compressive strengths of the specimens heated at 200 °C, 400 °C, and 600 °C were 96%, 73%, and 51%, respectively. The residual splitting tensile strength of geopolymer concrete specimens before and after subjected to various temperatures is shown in Figure 5-c. When exposed to different temperatures of 200 °C, 400 °C, and 600 °C, the residual splitting tensile strengths were 90%, 52%, and 30% for, respectively. As seen in Figure 5 (b and c), the strength values for specimens decreased slightly at 200 °C and significantly at 400 °C and 600 °C. The thermal pressure liberated by water evaporation from the geopolymer matrix may account for the observed drop in strength values as the temperature is increased in the specimens. As the temperature was raised, the vapor pressure grew, leading to thermal stresses that eventually led to the formation of thermal cracks [39].

**Table 5. Mechanical characteristics of geopolymer concrete**

| Temperature (℃) | Density, $\gamma_c$(Kg/m$^3$) | Compressive strength, fcu (MPa) | Splitting strength, ft (MPa) |
|---|---|---|---|
| 20 | 2307 | 78.61 | 4.21 |
| 200 | 2254 | 75.48 | 3.8 |
| 400 | 2193 | 57.37 | 2.21 |
| 600 | 2150 | 40.27 | 1.28 |

Note: The average strength was determined by testing three samples from each group.

### 3.2. Failure Mode

In order to illustrate the influence of the several key parameters of this study on failure modes, selected photos of specimens are shown in Figure 5. The failure modes of the geopolymer concrete specimens can be classified into three types, as shown in Figure 6: (1) CFRP sheet debonding, (2) concrete shear off, and (3) partial CFRP sheet rupture. It is worth noting that the geometric area of CFRP sheet and exposure temperature have the greatest influence on the failure modes of geopolymer concrete specimens. Specimens having a bonding area of Wf=50 mm and Lf=50 mm showed a CFRP-debonding failure mode at 20 and 200 °C, while at high temperatures of 400 and 600 °C, a concrete shear off was detected as shown in Figure 6-a. In specimens with a bonding area of Wf = 100 mm and Lf = 50 mm, concrete shear off was observed (Figure 6-b) for all specimens applied to various temperatures. The failure mode of specimens with Wf=50 mm and Lf=100 mm (Figure 6-c) exposed to 20, 200, and 400 °C was a partial rupture at the CFRP sheet; however, at 600 °C, a concrete shear off was seen. When the bonding area was large (Wf=100 mm and Lf=100 mm), the failure mode for all specimens tested at different temperatures was a concrete-shear off, as shown in Figure 6-d. According to the discussion above, the width and length of the CFRP bonding and the temperature conditions are the key determinants of the failure modes of specimens. It seems that when the bonding width and length were low, debonding of CFRP from the specimen surface occurred. In contrast, with the rise in temperature and an increase in both bonding width and length, concrete shear off was observed in the specimens. This observation indicates that the bond strength in these specimens surpasses the pull-off tensile strength of geopolymer concrete, as a larger portion of the concrete fractured and adhered to the surface of the CFRP sheet upon failure. A similar behavior has been reported in previous literature [31, 35–37, 32].

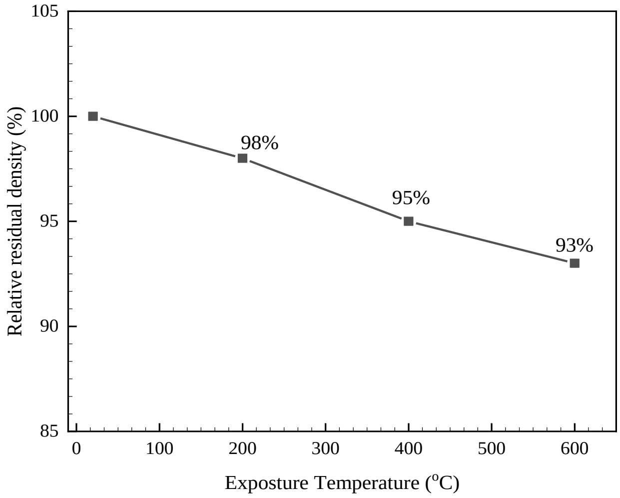


(a)

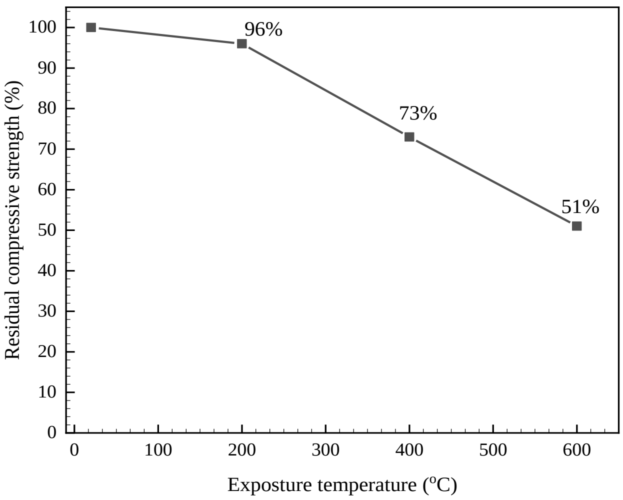


(b)

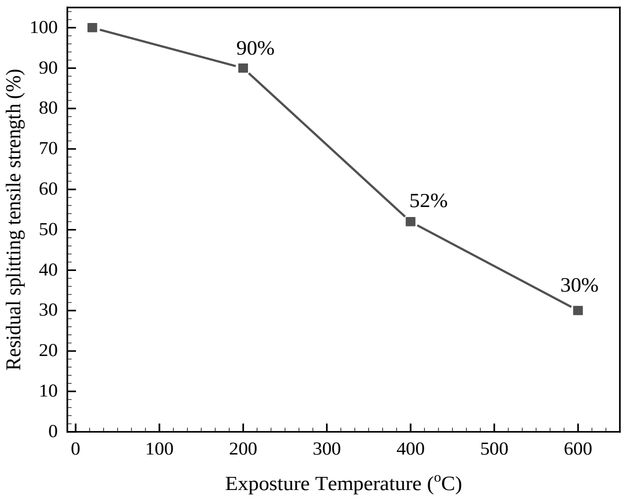


(c)

**Figure 5. Residual values of geopolymer concrete exposed to elevated temperatures (a) density, (b) compressive strength, and (c) splitting tensile strength**

20 °C

200 °C

400 °C

600 °C

**(a) Wf = 50 mm, Lf = 50 mm**

20 °C

200 °C

400 °C

600 °C

**(b) Wf = 100 mm, Lf = 50 mm**

20 °C

200 °C

400 °C

600 °C

**(c) Wf = 50 mm, Lf = 100 mm**

20 °C

200 °C

400 °C

600 °C

**(d) Wf = 100 mm, Lf = 100 mm**

**Figure 6. Failure modes of geopolymer concrete specimens**

### 3.3. Bond Force – Slippage Curves

The bond force-slippage responses of all specimens tested are presented in Figure 7. The bond force-slip curves for geopolymer concrete specimens show two distinct stages, as shown in Figure 7. However, specimens with an area of bonding of Wf=50 mm and Lf=100 mm exhibit three stages. The initial stage, representing the specimen's elastic behavior and stiffness, constitutes a linear zone that commences at the onset of the loading process. This zone extends until the point of CFRP sheet debonding initiation and is characterized by a gradual increase in bond force accompanied by a slight slip. This behavior is consistent across all samples tested. The second stage is nonlinear, starting at the end of the elastic zone and continuing until failure, where the bond force rises rapidly with a significant increase in slip. The behavior during this phase reflects the progressive debonding and failure of the bond between the CFRP sheet and the geopolymer concrete substrate [31, 35, 36].

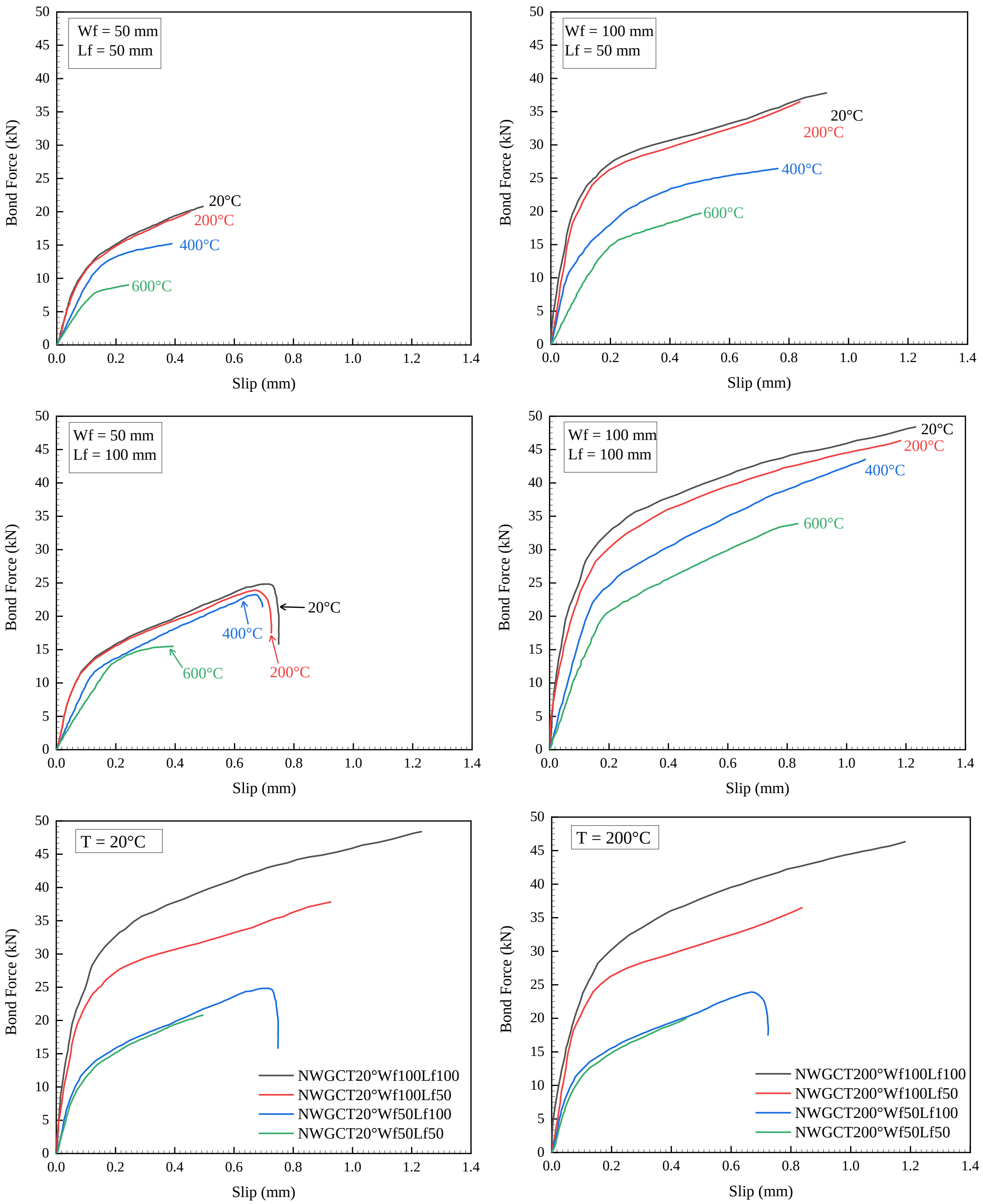

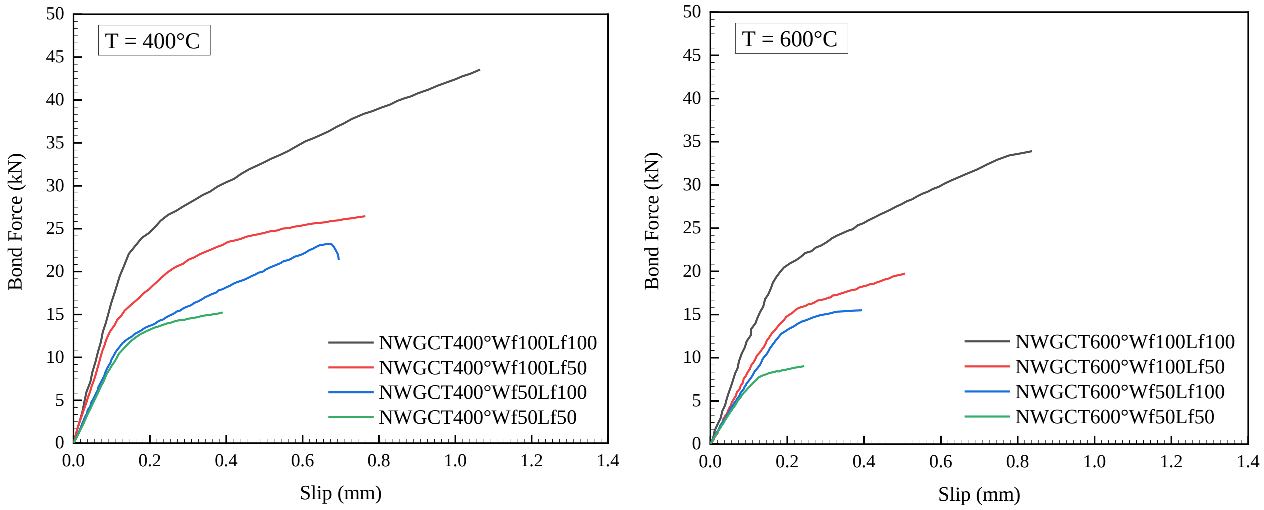


**Figure 7. Bond force vs. slippage curves of geopolymer concrete specimens**

Unlike other specimens, a specimen with an area of bonding of Wf=50 mm and Lf=100 mm shows an additional stage after reaching the ultimate load. After the ultimate load, the bond force drops rapidly while the slip remains constant, indicating partial rupture of the CFRP sheet. This rapid drop suggests a sudden loss of load-bearing capacity due to the failure of the CFRP sheet, which is a critical point for evaluating the durability and reliability of the bond in structural applications. This behavior is consistent with the findings in Irshidat & Al-Saleh (2016) study [31].

### 3.4. Maximum Bond Force and Ultimate Slip

The experimental results obtained from all specimens are summarized in Table 6. To investigate the effect of the CFRP bonding width and length on the bond-slip behavior at different temperatures, the maximum bond force ($P_{max}$) and ultimate slip ($S_u$) for each sample were compared to that of the sample with a smaller bonding area of Wf=50 mm and Lf=50 mm. As shown in Table 6 and Figure 7, both the maximum bond force and ultimate slip increased as the CFRP bonding area increased. For unheated specimens, the maximum bond force increased by 19%, 82%, and 133% when Wf and Lf were increased to (Wf=50 mm, Lf=100 mm), (Wf=100 mm, Lf=50 mm), and (Wf=100 mm, Lf=100 mm), respectively. Similarly, the ultimate slip increased by 51%, 87%, and 148%, respectively. The same trend was observed for specimens exposed to 200°C, where the improvement in both the maximum bond force and ultimate slip was approximately the same as for unheated specimens, indicating thermal stability up to this temperature. For specimens heated to 400°C, the maximum bond force improved by 52%, 74%, and 186% when the CFRP sheet was (Wf=50mm, Lf=100 mm), (Wf=100 mm, Lf=50 mm), and (Wf=100 mm, Lf=100 mm), respectively. Additionally, the ultimate slip increased by 77%, 95%, and 172%, respectively. Improvements in bond force and slip indicate substantial thermal resilience, though somewhat less than at lower temperatures. For specimens exposed to 600°C, an improvement in the maximum bond force of 72%, 119%, and 276%, respectively, was observed for the same parameters. Furthermore, the corresponding ultimate slip improved by 61%, 107%, and 242%, respectively. This indicates that larger bonding areas significantly counteract thermal degradation.

The aforementioned findings indicate that increasing the bonding area (Wf and Lf) of the CFRP significantly enhances both $P_{max}$ and $S_u$ across all temperatures. This can be attributed to the larger surface area allowing for better stress distribution and more effective load transfer between the CFRP and geopolymer concrete.

### 3.5. Impact of Exposure Temperature on the Behavior of Bond Force-Slip

Figure 8 displays the normalized values of the maximum bond force ($P_{max}$) and ultimate slip ($S_u$) for geopolymer concrete specimens subjected to various temperature exposures. The results of specimens with different bonding widths and lengths were compared to that of the control specimen, which was an unheated specimen. The results indicate that $P_{max}$ and $S_u$ decreased significantly with increasing exposure temperature for all tested specimens. This trend is consistent across all specimen types and sizes. Specifically, for a specimen with Wf=50mm and Lf=50mm (Figure 8-a), the maximum bond force decreased by 4%, 27%, and 57%, respectively, when exposed to higher temperatures of 200 °C, 400 °C, and 600 °C. Correspondingly, there was a 9%, 21%, and 51% decrease in the corresponding ultimate slippage, respectively. The small bonding area is more susceptible to high-temperature damage due to the limited bonding interface. Similarly, for a specimen with Wf=50 mm and Lf=100 mm, the reduction in maximum bond force when exposed to higher temperatures of 200 °C, 400 °C, and 600 °C was 4%, 7%, and 38%, respectively (Figure 8-b). Furthermore, the corresponding ultimate slippage decreased by 3%, 7%, and 47%, respectively. The increased length helps maintain better performance up to moderate temperatures. For a specimen with Wf=100 mm and Lf=50 mm, the reduction in the maximum bond force when exposed to higher temperatures of 200 °C, 400 °C, and 600 °C was 3%, 30%, and 48%, respectively (Figure 8-c). Additionally, the corresponding ultimate slippage decreased by 10%, 18%, and 45%, respectively. Increased width provides some thermal resilience but not as much as combined width and length.

For a specimen with Wf=100 mm and Lf=100 mm, the reduction in the maximum bond force when exposed to higher temperatures of 200 °C, 400 °C, and 600 °C was 4%, 10%, and 30%, respectively (Figure 8-d). Correspondingly, the corresponding ultimate slippage decreased by 4%, 14%, and 32%, respectively. The larger bonding area exhibits better resistance to thermal degradation compared to smaller bonding areas.

**Table 6. Tested results for specimens**

| Designation | T, ℃ | Wf, mm | Lf, mm | $P_{max}$, kN | $S_u$, mm | S, kN/mm | PR, % | EA, kN.mm | EAR, % |
|---|---|---|---|---|---|---|---|---|---|
| NWGCT20°Wf50Lf50 | 20 | 50 | 50 | 20.81 | 0.497 | 152 | 100 | 7.45 | 100 |
| NWGCT20°Wf50Lf100 | | 50 | 100 | 24.83 | 0.749 | 178 | 100 | 13.72 | 100 |
| NWGCT20°Wf100Lf50 | | 100 | 50 | 37.83 | 0.928 | 374 | 100 | 27.86 | 100 |
| NWGCT20°Wf100Lf100 | | 100 | 100 | 48.41 | 1.234 | 538 | 100 | 48.27 | 100 |
| NWGCT200°Wf50Lf50 | 200 | 50 | 50 | 20.08 | 0.452 | 146 | 96 | 6.40 | 86 |
| NWGCT200°Wf50Lf100 | | 50 | 100 | 23.93 | 0.724 | 172 | 97 | 12.79 | 93 |
| NWGCT200°Wf100Lf50 | | 100 | 50 | 36.52 | 0.838 | 278 | 74 | 23.67 | 85 |
| NWGCT200°Wf100Lf100 | | 100 | 100 | 46.37 | 1.184 | 488 | 91 | 43.68 | 90 |
| NWGCT400°Wf50Lf50 | 400 | 50 | 50 | 15.24 | 0.391 | 90 | 59 | 4.36 | 59 |
| NWGCT400°Wf50Lf100 | | 50 | 100 | 23.24 | 0.694 | 97 | 54 | 11.08 | 81 |
| NWGCT400°Wf100Lf50 | | 100 | 50 | 26.46 | 0.764 | 145 | 39 | 15.68 | 56 |
| NWGCT400°Wf100Lf100 | | 100 | 100 | 43.54 | 1.065 | 165 | 31 | 33.46 | 69 |
| NWGCT600°Wf50Lf50 | 600 | 50 | 50 | 9.03 | 0.245 | 72 | 47 | 1.54 | 21 |
| NWGCT600°Wf50Lf100 | | 50 | 100 | 15.49 | 0.395 | 77 | 43 | 4.32 | 31 |
| NWGCT600°Wf100Lf50 | | 100 | 50 | 19.75 | 0.506 | 83 | 22 | 7 | 25 |
| NWGCT600°Wf100Lf100 | | 100 | 100 | 33.92 | 0.838 | 124 | 23 | 20.22 | 42 |

$P_{max}$: bond force; Su: ultimate slip; S: stiffness; SR: stiffness retention; EA: energy absorption; EAR: energy absorption retention.

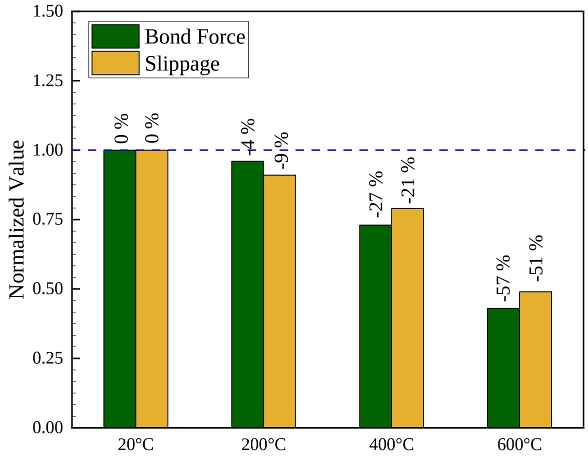


(a) Wf=50mm, Lf=50mm

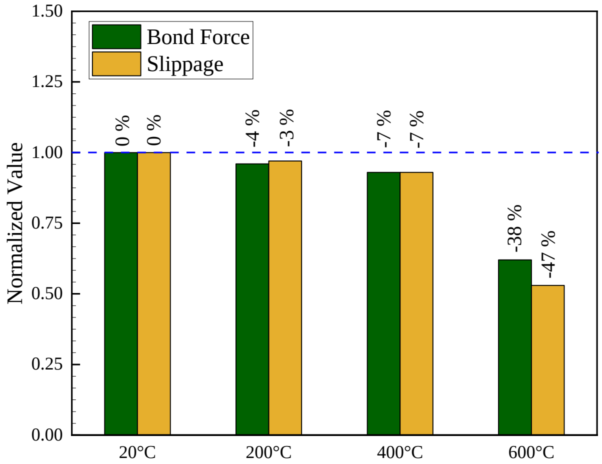


(b) Wf=50mm, Lf=100mm

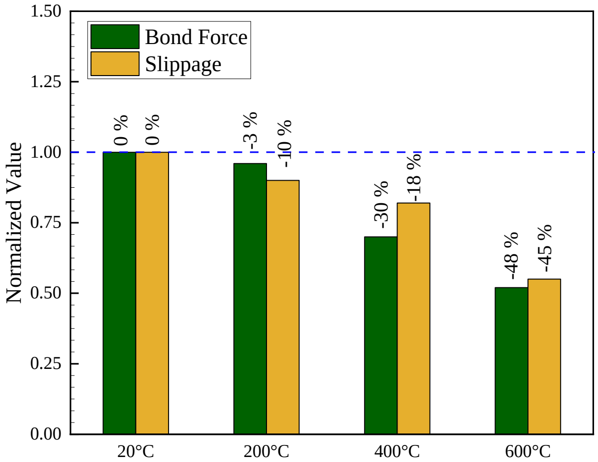


(c) Wf=100mm, Lf=50mm

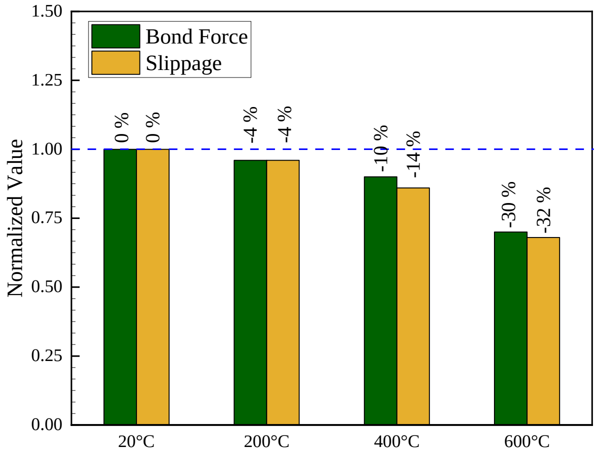


(d) Wf=100mm, Lf=100mm

**Figure 8. Normalized values of $P_{max}$ and $S_u$ with different temperatures for GCs specimens**

The aforementioned findings indicate that the maximum bond force and ultimate slip both decreased at temperatures reaching up to 400 °C. This decline can be attributed to the deterioration and reduction in mechanical strengths observed in the geopolymer concrete specimens at high temperatures.

### 3.6. Stiffness and Stiffness Retention

Tables 6 display the computation of stiffness and stiffness retention in relation to the bond-slippage curves of the geopolymer concrete specimens. The stiffness, represented by the slope of the initial stage of the curve, is determined by analyzing the response of specimens in their early stage. In contrast, stiffness retention measures the residual stiffness that remains in the specimens after they have been exposed to high temperatures. Figure 9-a depicts the stiffness results for geopolymer concrete specimens, which reveal an increase in stiffness values with an increase in CFRP bond width and length at the same temperature. This is because larger bonding areas provide better load distribution and adhesion, thereby increasing the resistance to initial deformation. However, these values decrease with an increase in temperature for the same CFRP configuration. This is due to the thermal degradation of the geopolymer matrix and the bonding interface, which reduces the material's structural integrity.

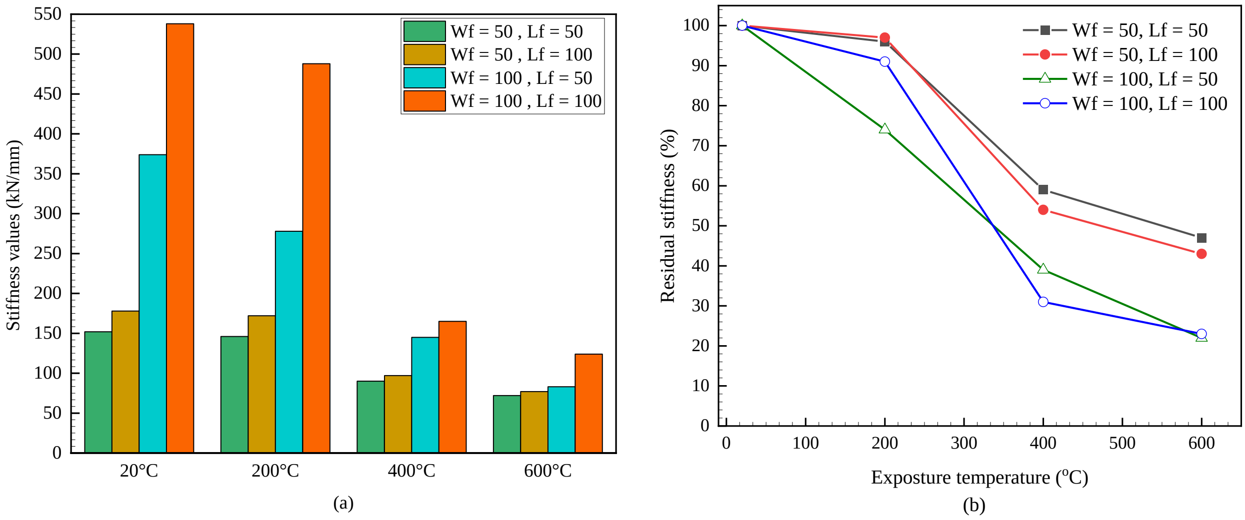


**Figure 9. Stiffness results of specimens (a) stiffness, (b) stiffness retention**

Control specimens displayed an increase in stiffness values by 17%, 146%, and 254% when Wf and Lf were increased to (Wf=50 mm, Lf=100 mm), (Wf=100 mm, Lf=50 mm), and (Wf=100 mm, Lf=100 mm), respectively. For specimens exposed to 200 °C, stiffness values increased by 17%, 90%, and 234% when Wf and Lf were increased to (Wf=50 mm, Lf=100 mm), (Wf=100 mm, Lf=50 mm), and (Wf=100 mm, Lf=100 mm), respectively. In other words, at low temperatures up to 200 °C, the stiffness values increase notably with larger bond areas, maintaining a significant portion of the initial stiffness. At 400°C, stiffness values increased by 8%, 61%, and 83% when the width and length were increased to (Wf=50 mm, Lf=100 mm), (Wf=100 mm, Lf=50 mm), and (Wf=100 mm, Lf=100 mm), respectively. At 600°C, specimens displayed an increase in stiffness values of 7%, 15%, and 72% when the width and length were increased to (Wf=50 mm, Lf=100 mm), (Wf=100 mm, Lf=50 mm), and (Wf=100 mm, Lf=100 mm), respectively. This indicated that at high temperatures ranging from 400°C to 600°C, the increase in stiffness with bond area becomes less pronounced, indicating that the benefits of larger bond areas diminish at higher temperatures due to extensive thermal degradation.

The stiffness retention due to high temperatures is also illustrated in Figure 9-b, where the average residual stiffness values for specimens exposed to 200°C, 400°C, and 600°C were 89%, 46%, and 34%, respectively. This decline highlights the severe impact of high temperatures on the mechanical properties of geopolymer concrete.

### 3.7. Energy-Absorption and Energy-Absorption Retention

Energy-absorption and energy-absorption retention calculations for the specimens are shown in Tables 6. Energy-absorption is obtained by calculating the total area under bond-slippage curves, and energy-absorption retention is the remaining energy absorbed by the specimens after being exposed to high temperatures. The energy absorption values of specimens for various CFRP configurations are depicted in Figure 10-a, and it is evident that, for the same temperature, the values increased as the width and length of the CFRP bond increased. This indicates that larger bonding areas provide better load distribution and increase the energy dissipation capacity. However, these values decreased with increasing temperature.

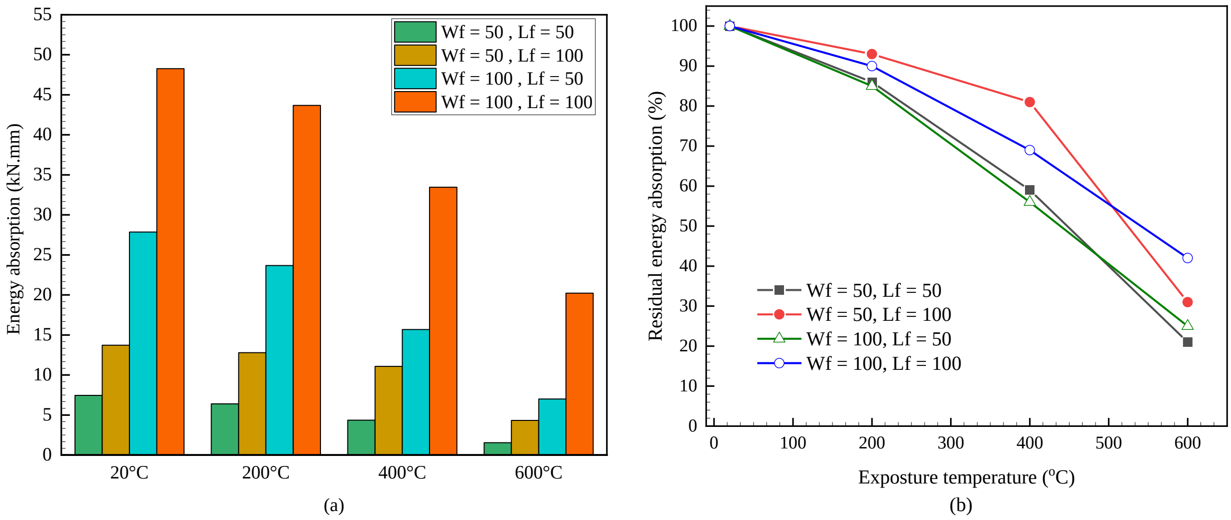


**Figure 10. Energy absorption results (a) energy-absorption, (b) energy-absorption retention**

The energy absorption values for unheated specimens increased by 84%, 274%, and 548% as the width and length of the CFRP bond were increased to (Wf=50 mm, Lf=100 mm), (Wf=100 mm, Lf=50 mm), and (Wf=100 mm, Lf=100 mm), respectively. Similarly, the energy absorption values for specimens exposed to 200 °C increased by 100%, 270%, and 583%, while those exposed to 400 °C increased by 154%, 260%, and 667% for the aforementioned CFRP configurations. Specimens exposed to 600 °C exhibited a significant increase in energy absorption values of 181%, 355%, and 1213% for the respective CFRP configurations. These significant increases, especially at higher temperatures, indicate that while overall energy absorption decreases with temperature, larger bond areas still significantly improve performance.

The energy-absorption retention of the specimens with increasing temperature is also depicted in Figure 10-b, and the average residual of the energy absorption for specimens when exposed to 200 °C, 400 °C, and 600 °C was 89%, 66%, and 30%, respectively. This highlights the substantial loss in energy absorption capacity at higher temperatures, emphasizing the need for materials with better thermal stability in high-temperature applications.

### 3.8. Proposed Model of Mechanical Properties and Bond-Slippage

Several models have been proposed for the prediction of the compressive strength and tensile strength of concrete after being exposed to elevated temperatures. The Eurocode model [40] is currently the most popular among these proposals. The compressive strength and tensile strength could be estimated in term of exposed temperatures (T) according to Eurocode as follow:

$$\mathrm{f}_{\mathrm{c,T}} = f_{c,20^\circ}\begin{cases}1 & T \leq 100°C\\ 1.067 - 0.00067T & 100°C \leq T \leq 400°C\\ 1.44 - 0.0016T & T \geq 400°C\end{cases} \tag{1}$$

$$f_{t,T} = f_{t,20^\circ}\begin{cases}1 & T \leq 100°C\\ 1 - \frac{T-100}{500} & 100°C \leq T \leq 600°C\end{cases} \tag{2}$$

In this study, a linear regression analysis was used to predict the compressive and tensile strength of specimens subjected to exposure temperatures (T) according to the following equations:

$$\mathrm{f}_{\mathrm{c,GC,T}} = \mathrm{f}_{\mathrm{c,20^\circ}}\begin{cases}1.0044 - 0.00022T & T \leq 200°C\\ 1.0275 - 0.000824T & 200°C < T \leq 600°C\end{cases} \tag{3}$$

$$f_{t,GC,T} = f_{t,20^\circ}\begin{cases}1.011 - 0.00054T & T \leq 200°C\\ 1.02 - 0.0012T & 200°C < T \leq 600°C\end{cases} \tag{4}$$

where $f_{c,20°C}$, and $f_{t,20°C}$ represent the compressive and tensile strength of geopolymer concrete at ambient room temperature. Figure 11 shows the normalized values of compressive and tensile strengths of specimens obtained by the proposed equations and those expressed by Eurocode. As shown in Figure 11, the proposed equations show a good fit with experimental data and are close to the values obtained from Eurocode.

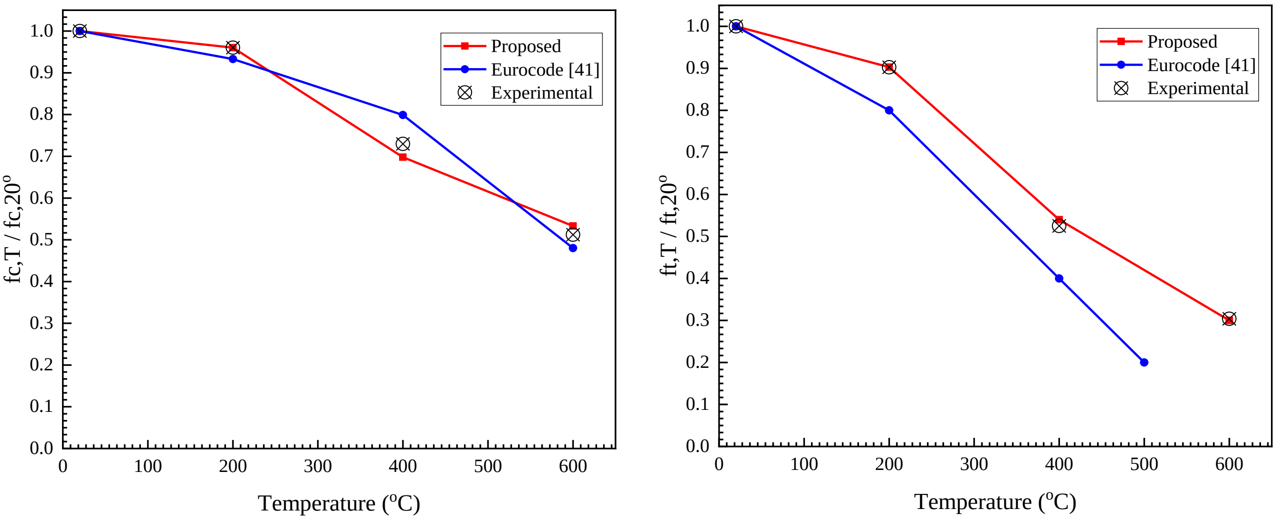


**Figure 11. Normalized compressive and tensile strengths of experimental, proposed and Eurocode [40]**

A bond-slip model had been proposed by Alshuqari & Çevik [37] to predict the maximum bond force ($P_{max}$) and corresponding ultimate slippage ($S_u$), which consider the strengths of geopolymer concrete, the geometric and mechanical characteristics of FRP sheets, and the effect of end groove anchorage. In this study, this model has been used after incorporating a factor ($\alpha_t$) that considers the exposure temperature effect on the bond-slippage behavior as follows:

$$P_{max} = \alpha_{t,P}\left[1.9935e^{-6} f_{cu} f_t + 0.1196 W_f L_f^{0.0001308\gamma_c}\right] \quad (5)$$

$$S_u = \alpha_{t,S}\left[1.46e^{-10} W_f L_f^{0.5} \gamma_c^2 \frac{\sqrt{fcu/ft}}{ft}\right] \quad (6)$$

where $f_{cu}$, $f_t$, and $\gamma_c$ represent the mechanical properties of geopolymer concrete (compressive strength, tensile strength, and density) respectively, $W_f$ is the CFRP bonding width, and $L_f$ is the CFRP bonding length. The αt factor of geopolymer concrete specimens exposed to elevated temperatures (T) for bond force and slippage is expressed as:

$$\alpha_{t,P} = 1 + 7.33e^{-5}T - 1.314e^{-6}T^2 \quad (7)$$

$$S_u = \alpha_{t,S}\left[1.46e^{-10} W_f L_f^{0.5} \gamma_c^2 \frac{\sqrt{fcu/ft}}{ft}\right] \quad (8)$$

Figure 12 compares the bonding force and slippage values obtained experimentally with those predicted by the proposed model for geopolymer concrete specimens. The R-squared values for bond force and slippage, as shown in Figure 12, were found to be 91% and 87%, respectively. These values show a good overall fit for the proposed model, considering various factors such as the type of geopolymer concrete, varying bonding length and width values, and varying exposure temperature values. Table 7 summarizes the results of the tested data and the values derived by the proposed model for specimens. The average ratios of $P_{max,test}/P_{max,predicted}$ and $S_{u,test}/S_{u,predicted}$ were 1.02 and 1.1 ,respectively, demonstrating that the proposed model yields acceptable results and is suitable for practical implementations.

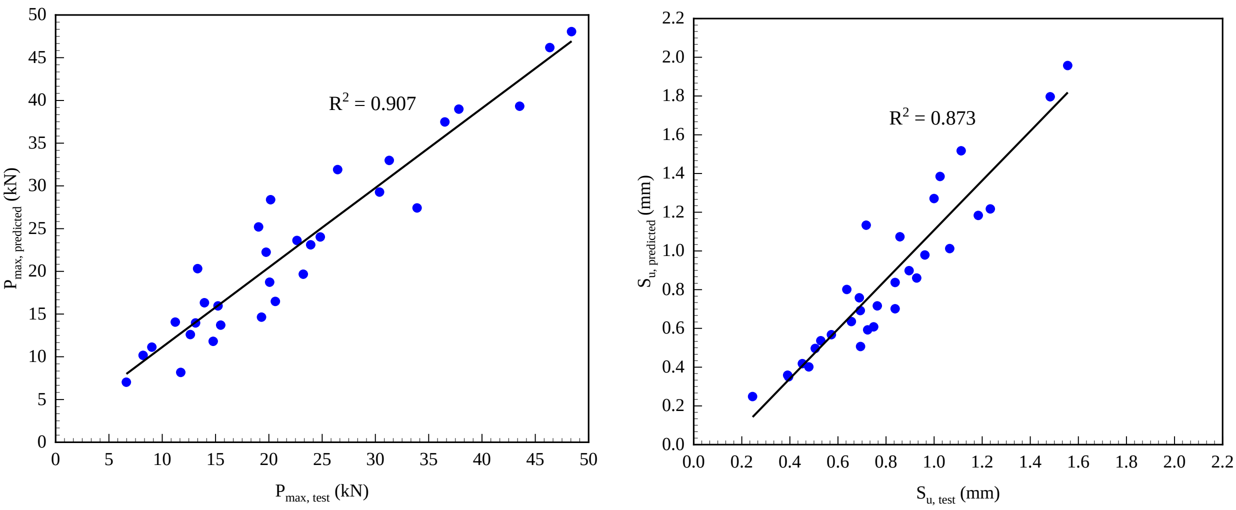


**Figure 12. Tested vs predicted bond force and slippage of specimens**

**Table 7. Tested and predicted results of bond-slippage for specimens**

| Designation | $P_{max,test,}$ kN | $P_{max,predicted}$ kN | $P_{max,test}$ / $P_{max,predicted}$ | $S_{u,test}$ mm | $S_{u,predicted}$ mm | $S_{u,test}$ / $S_{u,predicted}$ |
|---|---|---|---|---|---|---|
| NWGCT20°Wf50Lf50 | 20.81 | 19.49 | 1.07 | 0.497 | 0.430 | 1.16 |
| NWGCT20°Wf50Lf100 | 24.83 | 24.02 | 1.03 | 0.749 | 0.608 | 1.23 |
| NWGCT20°Wf100Lf50 | 37.83 | 38.98 | 0.97 | 0.928 | 0.860 | 1.08 |
| NWGCT20°Wf100Lf100 | 48.41 | 48.05 | 1.01 | 1.234 | 1.217 | 1.01 |
| NWGCT200°Wf50Lf50 | 20.08 | 18.73 | 1.07 | 0.452 | 0.418 | 1.08 |
| NWGCT200°Wf50Lf100 | 23.93 | 23.09 | 1.04 | 0.724 | 0.592 | 1.22 |
| NWGCT200°Wf100Lf50 | 36.52 | 37.47 | 0.97 | 0.838 | 0.837 | 1.00 |
| NWGCT200°Wf100Lf100 | 46.37 | 46.18 | 1.00 | 1.184 | 1.183 | 1.00 |
| NWGCT400°Wf50Lf50 | 15.24 | 15.95 | 0.96 | 0.391 | 0.358 | 1.09 |
| NWGCT400°Wf50Lf100 | 23.24 | 19.66 | 1.18 | 0.694 | 0.506 | 1.37 |
| NWGCT400°Wf100Lf50 | 26.46 | 31.90 | 0.83 | 0.764 | 0.716 | 1.07 |
| NWGCT400°Wf100Lf100 | 43.54 | 39.32 | 1.11 | 1.065 | 1.012 | 1.05 |
| NWGCT600°Wf50Lf50 | 9.03 | 11.12 | 0.81 | 0.245 | 0.248 | 0.99 |
| NWGCT600°Wf50Lf100 | 15.49 | 13.70 | 1.13 | 0.395 | 0.350 | 1.13 |
| NWGCT600°Wf100Lf50 | 19.75 | 22.23 | 0.89 | 0.506 | 0.496 | 1.02 |
| NWGCT600°Wf100Lf100 | 33.92 | 27.41 | 1.24 | 0.838 | 0.701 | 1.20 |
| Average | | | 1.02 | | | 1.1 |

## 3.9. SEM Analysis

The SEM images of geopolymer concrete specimens exposed to temperatures of 20, 200, 400, and 600 °C are presented in Figure 13. As displayed in Figure 13-b, the microstructure of specimens heated at 200 °C appears similar to that of unheated specimens, indicating that the specimen remains unaffected at temperatures below 200 °C. Consequently, the mechanical characteristics and bond-slip behavior of specimens heated at 200 °C are comparable to those of unheated specimens. Conversely, high-temperature exposure results in binder microstructure degradation and micro and thermal cracks in specimens, as shown in Figure 13-c and Figure 13-d. The SEM image of the sample heated to 600 °C exhibits a higher level of microstructure binder deterioration, with an increase in micro-crack propagation and thermal crack size. The deterioration and crack growth, which deteriorate mechanical strengths and bond-slip characteristics, may be attributed to thermal stress caused by water evaporation from the geopolymer matrix during heating.

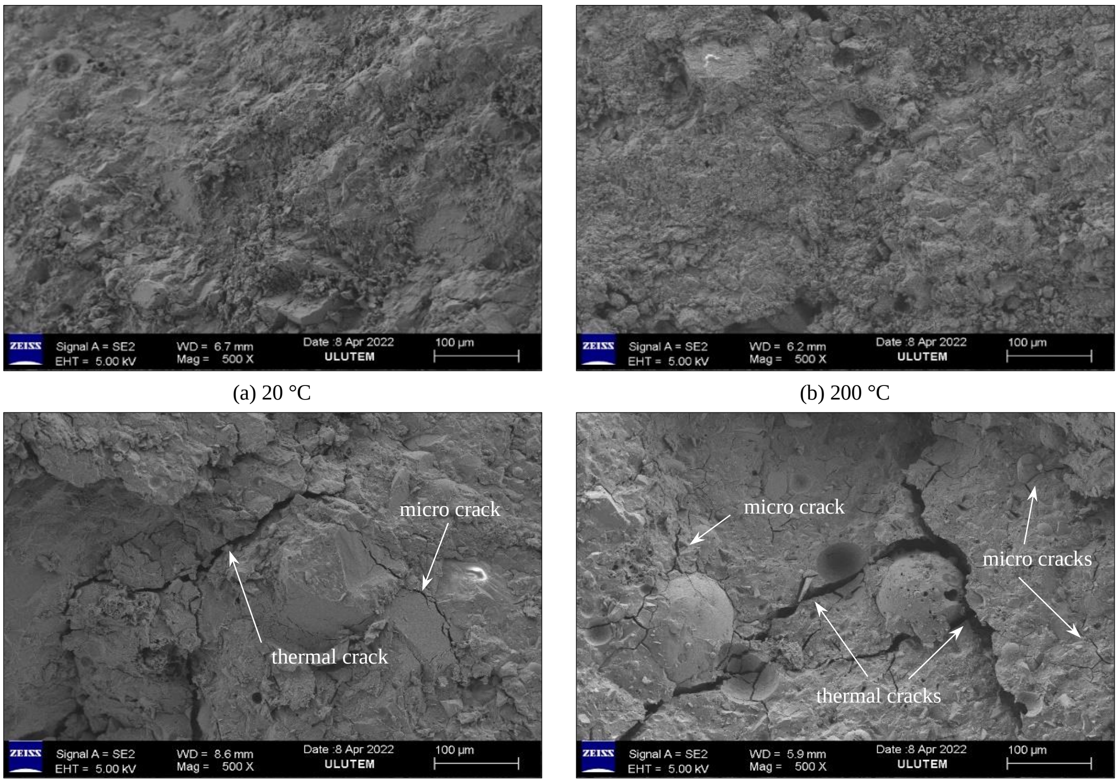


(a) 20 °C (b) 200 °C

(c) 400 °C (d) 600 °C

**Figure 13. SEM micrographs of geopolymer concrete specimens**

## 4. Conclusions

In this study, the bond-slip behavior between CFRP sheets and heat-damaged geopolymer concrete specimens was examined. The bond-slip characteristics were assessed with specimens measuring of 150x150x150mm, with consideration given to varying factors such as elevated temperatures (20°C, 200°C, 400°C, and 600°C), CFRP bonding width (Wf) of 50 and 100mm, and CFRP bonding length (Lf) of 50 and 100mm. To conduct the study, geopolymer concrete samples were cast, heated to elevated temperatures, bonded to the relevant CFRP sheets, and then subjected to a double-shear test. The following conclusions can be made based on the experimental findings of this study:

- Exposure to high temperatures resulted in a decrease in mechanical strength characteristics. A slight reduction in compressive strengths was observed at low temperatures up to 200 °C, whereas at higher temperatures up to 600 °C, the residual compressive and splitting strengths of specimens were 51% and 30%, respectively.
- The failure mode of the specimens was determined based on the exposure temperature conditions. Moreover, the failure mode of geopolymer concrete specimens varied depending on the length and width of the CFRP bonding. Three different failure modes were observed in specimens: concrete rupture, partial rupture of the CFRP sheet, and CFRP debonding.
- Greater bond force and slip were seen as the CFRP sheet bonding area was increased. However, for the same area bonding (Wf and Lf), increasing Wf had a more significant effect on the bond-slip relationship for specimens than increasing Lf.
- The bond-slip behavior of specimens after exposure to high temperatures up to 400 and 600 °C considerably degraded in comparison to those exposed to low temperatures up to 200 °C. At 200 °C, the bond force and corresponding slippage of specimens declined by an average of 5%.
- The bond force and associated slippage decreased to 17% and 15%, respectively, for specimens, when subjected to a temperature of 400 °C. Moreover, at 600 °C, the average results of the bond force and corresponding slippage of specimens were reduced by 42% and 47%, respectively.
- The SEM analysis revealed that the specimens are unaffected at low temperatures; however, exposure to high temperatures causes the binder's microstructure to deteriorate.

The proposed model, which was developed to predict the maximum bond force ($P_{max}$) and associated ultimate slippage ($S_u$) for the specimens, showed good agreement with the tested results.

## 5. Declarations

### 5.1. Author Contributions

Conceptualization, E.A.A. and A.C.; methodology, E.A.A.; software, E.A.A.; validation, E.A.A.; investigation, E.A.A.; data curation, E.A.A.; writing—original draft preparation, E.A.A.; writing—review and editing, A.C.; supervision, A.C. All authors have read and agreed to the published version of the manuscript.

### 5.2. Data Availability Statement

The data presented in this study are available in the article.

### 5.3. Funding

The authors received no financial support for the research, authorship, and/or publication of this article.

### 5.4. Conflicts of Interest

The authors declare no conflict of interest.

## 6. References

[1] Behera, M., Bhattacharyya, S. K., Minocha, A. K., Deoliya, R., & Maiti, S. (2014). Recycled aggregate from C&D waste & its use in concrete - A breakthrough towards sustainability in construction sector: A review. Construction and Building Materials, 68, 501–516. doi:10.1016/j.conbuildmat.2014.07.003.

[2] Davidovits, J. (1994). Global warming impact on the cement and aggregates industries. World Resource Review, 6(2), 263-278.

[3] Chen, J., Shen, L., Song, X., Shi, Q., & Li, S. (2017). An empirical study on the CO2 emissions in the Chinese construction industry. Journal of Cleaner Production, 168, 645–654. doi:10.1016/j.jclepro.2017.09.072.

[4] Davidovits, J. (1989). Geopolymers and geopolymeric materials. Journal of Thermal Analysis, 35(2), 429–441. doi:10.1007/BF01904446.

[5] Davidovits, J. (1991). Geopolymers - Inorganic polymeric new materials. Journal of Thermal Analysis, 37(8), 1633–1656. doi:10.1007/BF01912193.

[6] Tanyildizi, H., & Yonar, Y. (2016). Mechanical properties of geopolymer concrete containing polyvinyl alcohol fiber exposed to high temperature. Construction and Building Materials, 126, 381–387. doi:10.1016/j.conbuildmat.2016.09.001.

[7] Ramujee, Kolli., & PothaRaju, M. (2017). Mechanical Properties of Geopolymer Concrete Composites. Materials Today: Proceedings, 4(2), 2937–2945. doi:10.1016/j.matpr.2017.02.175.

[8] Szabó, R., Dolgos, F., Debreczeni, Á., & Mucsi, G. (2022). Characterization of mechanically activated fly ash-based lightweight geopolymer composite prepared with ultrahigh expanded perlite content. Ceramics International, 48(3), 4261–4269. doi:10.1016/j.ceramint.2021.10.218.

[9] Tale Masoule, M. S., Bahrami, N., Karimzadeh, M., Mohasanati, B., Shoaei, P., Ameri, F., & Ozbakkaloglu, T. (2022). Lightweight geopolymer concrete: A critical review on the feasibility, mixture design, durability properties, and microstructure. Ceramics International, 48(8), 10347–10371. doi:10.1016/j.ceramint.2022.01.298.

[10] Luhar, S., Nicolaides, D., & Luhar, I. (2021). Fire Resistance Behaviour of Geopolymer Concrete: An Overview. Buildings, 11(3), 82. doi:10.3390/buildings11030082.

[11] Abd Razak, S. N., Shafiq, N., Guillaumat, L., Farhan, S. A., & Lohana, V. K. (2022). Fire-Exposed Fly-Ash-Based Geopolymer Concrete: Effects of Burning Temperature on Mechanical and Microstructural Properties. Materials, 15(5), 1884. doi:10.3390/ma15051884.

[12] Cao, V. D., Pilehvar, S., Salas-Bringas, C., Szczotok, A. M., Rodriguez, J. F., Carmona, M., Al-Manasir, N., & Kjøniksen, A. L. (2017). Microencapsulated phase change materials for enhancing the thermal performance of Portland cement concrete and geopolymer concrete for passive building applications. Energy Conversion and Management, 133, 56–66. doi:10.1016/j.enconman.2016.11.061.

[13] Mane, S., & Jadhav, H. (2012). Investigation of geopolymer mortar and concrete under high temperature. Magnesium, 1(5), 384-390.

[14] Hassan, A., Arif, M., & Shariq, M. (2020). Mechanical Behaviour and Microstructural Investigation of Geopolymer Concrete After Exposure to Elevated Temperatures. Arabian Journal for Science and Engineering, 45(5), 3843–3861. doi:10.1007/s13369-019-04269-9.

[15] Mohmmad, S. H., Gülşan, M. E., & Çevik, A. (2022). Behaviour of Geopolymer Concrete Two-Way Slabs Reinforced by FRP Bars After Exposure to Elevated Temperatures. Arabian Journal for Science and Engineering, 47(10), 12399–12421. doi:10.1007/s13369-021-06411-y.

[16] Kadhim, S., Çevik, A., Niş, A., Bakbak, D., & Aljanabi, M. (2022). Mechanical behavior of fiber reinforced slag-based geopolymer mortars incorporating artificial lightweight aggregate exposed to elevated temperatures. Construction and Building Materials, 315. doi:10.1016/j.conbuildmat.2021.125766.

[17] Trentin, C., & Casas, J. R. (2015). Safety factors for CFRP strengthening in bending of reinforced concrete bridges. Composite Structures, 128, 188–198. doi:10.1016/j.compstruct.2015.03.048.

[18] Chen, W., Pham, T. M., Sichembe, H., Chen, L., & Hao, H. (2018). Experimental study of flexural behaviour of RC beams strengthened by longitudinal and U-shaped basalt FRP sheet. Composites Part B: Engineering, 134, 114–126. doi:10.1016/j.compositesb.2017.09.053.

[19] Al-Rousan, R. Z., Alhassan, M. A., & AlShuqari, E. A. (2018). Behavior of plain concrete beams with DSSF strengthened in flexure with anchored CFRP sheets—Effects of DSSF content on the bonding length of CFRP sheets. Case Studies in Construction Materials, 9, e00195. doi:10.1016/j.cscm.2018.e00195.

[20] Al-Abdwais, A. H. (2023). Experimental and Numerical Assessment of Bonding Between Geopolymer Concrete and CFRP Sheet Using NSM Techniques. Civil and Environmental Engineering, 19(2), 676–691. doi:10.2478/cee-2023-0061.

[21] Lei, M., Wang, X., Chen, J., Huang, H., Lin, J., Yan, Z., & Wu, Z. (2024). Bond behavior of the FRP grid-concrete interface with geopolymer mortar as an adhesive. Journal of Building Engineering, 87, 109120. doi:10.1016/j.jobe.2024.109120.

[22] Li, W., Li, S., Lu, Y., & Liu, Z. (2024). Bond properties of steel bar with engineered geopolymer composites under monotonic load. Structural Concrete, 1-23. doi:10.1002/suco.202300689.

[23] Khan, Q. S., Akbar, H., Qazi, A. U., Kazmi, S. M. S., & Munir, M. J. (2024). Bond Stress Behavior of a Steel Reinforcing Bar Embedded in Geopolymer Concrete Incorporating Natural and Recycled Aggregates. Infrastructures, 9(6), 93. doi:10.3390/infrastructures9060093.

[24] Niyazuddin, & Umesh, B. (2024). Experimental investigation on bond behaviour of the GFRP bars with normal and high strength geopolymer concrete. Construction and Building Materials, 429, 136395. doi:10.1016/j.conbuildmat.2024.136395.

[25] Zhao, J., Wang, S., Wang, Z., Wang, K., & Fu, C. (2023). Bond performance between FRP bars and geopolymer concrete after elevated temperature exposure. Construction and Building Materials, 384, 131476. doi:10.1016/j.conbuildmat.2023.131476.

[26] Nakaba, K., Kanakubo, T., Furuta, T., & Yoshizawa, H. (2001). Bond behavior between fiber-reinforced polymer laminates and concrete. ACI Structural Journal, 98(3), 359–367. doi:10.14359/10224.

[27] Mensah, C., Wang, Z., Bonsu, A. O., & Liang, W. (2020). Effect of different bond parameters on the mechanical properties of FRP and concrete interface. Polymers, 12(11), 2466. doi:10.3390/polym12112466.

[28] Ben Ouezdou, M., Belarbi, A., & Bae, S.-W. (2009). Effective Bond Length of FRP Sheets Externally Bonded to Concrete. International Journal of Concrete Structures and Materials, 3(2), 127–131. doi:10.4334/ijcsm.2009.3.2.127.

[29] Hosseini, A., & Mostofinejad, D. (2014). Effective bond length of FRP-to-concrete adhesively-bonded joints: Experimental evaluation of existing models. International Journal of Adhesion and Adhesives, 48, 150–158. doi:10.1016/j.ijadhadh.2013.09.022.

[30] Wang, H. T., Liu, S. S., Liu, Q. L., Pang, Y. Y., & Shi, J. W. (2021). Influences of the joint and epoxy adhesive type on the CFRP-steel interfacial behavior. Journal of Building Engineering, 43, 103167. doi:10.1016/j.jobe.2021.103167.

[31] Irshidat, M. R., & Al-Saleh, M. H. (2016). Effect of using carbon nanotube modified epoxy on bond-slip behavior between concrete and FRP sheets. Construction and Building Materials, 105, 511–518. doi:10.1016/j.conbuildmat.2015.12.183.

[32] Alhassan, M. A., Al Rousan, R. Z., & Al Shuqari, E. A. (2019). Bond-slip behavior between fiber reinforced concrete and CFRP composites. Ain Shams Engineering Journal, 10(2), 359–367. doi:10.1016/j.asej.2019.03.001.

[33] Al-Rousan, R. Z., & AL-Tahat, M. F. (2019). Consequence of surface preparation techniques on the bond behavior between concrete and CFRP composites. Construction and Building Materials, 212, 362–374. doi:10.1016/j.conbuildmat.2019.03.299.

[34] Haddad, R. H., & Al-Rousan, R. Z. (2016). An anchorage system for CFRP strips bonded to thermally shocked concrete. International Journal of Adhesion and Adhesives, 71, 10–22. doi:10.1016/j.ijadhadh.2016.08.003.

[35] Al-Rousan, R., & Al-Tahat, M. (2020). An anchoring groove technique to enhance the bond behavior between heat-damaged concrete and CFRP composites. Buildings, 10(12), 232. doi:10.3390/buildings10120232.

[36] Haddad, R. H., Al-Rousan, R., & Almasry, A. (2013). Bond-slip behavior between carbon fiber reinforced polymer sheets and heat-damaged concrete. Composites Part B: Engineering, 45(1), 1049–1060. doi:10.1016/j.compositesb.2012.09.010.

[37] Alshuqari, E. A., & Çevik, A. (2022). Behavior of bond-slip relationship of lightweight and normal weight geopolymer with various FRP sheets using end-groove anchorage. Construction and Building Materials, 343. doi:10.1016/j.conbuildmat.2022.128060.

[38] Alhamad, A., Yehia, S., Lublóy, É., & Elchalakani, M. (2022). Performance of Different Concrete Types Exposed to Elevated Temperatures: A Review. Materials, 15(14), 5032. doi:10.3390/ma15145032.

[39] Turkey, F. A., Beddu, S. B., Ahmed, A. N., & Al-Hubboubi, S. K. (2022). Effect of high temperatures on the properties of lightweight geopolymer concrete based fly ash and glass powder mixtures. Case Studies in Construction Materials, 17, 1489. doi:10.1016/j.cscm.2022.e01489.

[40] BS EN 1992-1-2:2004. (2004). Design of concrete structures - Part 1-2: General rules - Structural fire design. British Standard Institute (BSI), London, United Kingdom.